RESEARCH ARTICLE

Key Points:
- F_3 layer occurred over a large latitudinal extent from 20°S to 25°N dip latitudes during 17 March 2015 storm-induced PPEF phases
- The PPEF-generated superfountain led to the F_3 layer occurrence earlier at the equator and later at higher latitudes in both hemispheres
- F_3 layer was more distinct and stronger and lasted longer in the Northern Hemisphere due to the storm time asymmetric equatorward neutral winds

Correspondence to:
K. Venkatesh,
venkatkau@gmail.com

Superfountain Effect Linked With 17 March 2015 Geomagnetic Storm Manifesting Distinct F_3 Layer

K. Venkatesh[1] , A.K. Patra[1] , N. Balan[2], P.R. Fagundes[3] , S. Tulasi Ram[4], I.S. Batista[5] , and B.W. Reinisch[6]

[1]National Atmospheric Research Laboratory, Gadanki, India, [2]Institute of Space Sciences, Shandong University, Weihai, China, [3]IP&D, Universidade do Vale do Paraiba, São Paulo, Brazil, [4]Indian Institute of Geomagnetism, Navi Mumbai, India, [5]Instituto Nacional de Pesquisas Espaciais, São Paulo, Brazil, [6]Lowell Digisonde International, Lowell, MA, USA

Abstract The existence of an additional stratification in the daytime equatorial ionospheric F region (the F_3 layer) was known since the 1940s. However, its characteristics and the underlying physical mechanism have been uncovered only recently. In this paper, we present and discuss the F_3 layer characteristics observed by six ionosondes distributed over equatorial and low latitudes (−20° to +25° dip latitudes) in the Brazilian longitude sector during the strongest geomagnetic storm (DstMin = −223 nT) of solar cycle 24, the St. Patrick's Day storm of 17 March 2015. Two eastward prompt penetration electric field (PPEF) events, as seen in equatorial electrojet, occurred during the main phase of the storm on 17 March 2015, a strong one (~100 nT) at around ~1200 UT and a weak one (~50 nT) at around ~1725 UT. Local time variations in the F_3 layer occurrence and ionospheric base height (h′F), peak height (hmF), and peak electron density (Nmax) are investigated. Notably, the F_3 layer occurred at all six locations, more distinctly during the stronger PPEF event. The large latitudinal extend in the occurrence of the F_3 layer in opposite hemispheres (−20° to +25° dip latitudes) covering the equatorial ionization anomaly crests observed for the first time is interpreted in terms of the combined effect of the super plasma fountain generated by the eastward PPEF and storm time equatorward neutral wind.

1. Introduction

Geomagnetic storms affecting the equatorial ionosphere have been a subject of intense investigation in recent years. While many studies have dealt with the total electron content and F layer critical frequency (f_oF_2) variations, changes in the height distribution of electron density in response to the geomagnetic storm have been less addressed. Given the fact that the storms can modify the equatorial zonal electric field and the equatorial ionospheric height distribution of electron density is heavily governed by the zonal electric field, it is important to examine the vertical electron density distribution during the geomagnetic storms.

With regard to the equatorial ionosphere, it is well known that an additional layer, known as F_3 layer (Balan et al., 1997; Jenkins et al., 1997), can sometimes be generated. This additional layer does not occur at middle and high latitudes. Several research groups have published interesting papers on the formation mechanism and short- and long-term variations of the F_3 layer (Balan et al., 1998, 2000; Batista et al., 2002; Fagundes et al., 2007; Lynn et al., 2000; Rama Rao et al., 2005; Sreeja et al., 2010; Tardelli et al., 2016, 2018; Thampi et al., 2007; Uemoto et al., 2007, 2011; Zain et al., 2008; Zhao et al., 2014). As proposed by Balan et al. (1998), the F_3 layer occurs because of the combined effects of the upward $E \times B$ drift and magnetic meridional neutral wind together with the usual daytime photochemical and dynamical processes.

Given the fact that geomagnetic storms can alter equatorial electric field through prompt penetration electric field (PPEF; Zhao et al., 2005; Paznukhov et al., 2007; Lin et al., 2009; Sreeja et al., 2010; Klimenko et al., 2011), it is interesting to examine the response of the equatorial electron density profile, especially the formation of the F_3 layer, if any, by magnetic storms. In fact, Balan et al. (2008) studied the characteristics of F_3 layer occurrence during strong geomagnetic storm periods at equatorial locations in Brazilian, Indian, and Australian longitudes using observations and modeling and suggested that a strong and distinct F_3 layer during the main phase (MP) of geomagnetic storms could be formed by a strong eastward PPEF.

During the St. Patrick's Day storm of 17 March 2015, which is the strongest storm in the 24th solar cycle, the Brazilian sector was on the dayside, facilitating investigation of the storm time characteristics of
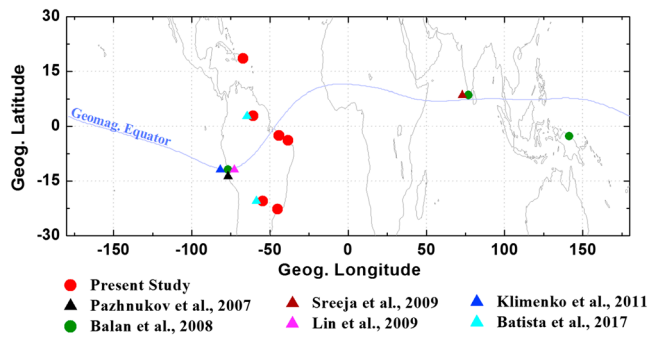
Figure 1. Map showing the geographic locations of the six ionosonde stations (red dots) used in the present study for the onset and evolution of F_3 layer during the geomagnetic storm of 17 March 2015. The locations of previous F_3 layer observations during geomagnetic storms are also shown. At the locations where more than one study exists, the filled circles represent exact location of the ionosondes, while the triangles are slightly shifted for visibility without overlapping.

several daytime equatorial phenomena including the F_3 layer (Batista et al., 2017; Kuai et al., 2016). Here, we focus on studying the effect of this intense geomagnetic storm in modifying the ionospheric vertical structure and especially the latitudinal and hemispheric differences in the formation of storm time F_3 layer. We carry out this study using simultaneous observations from six ionosondes distributed over a large latitudinal range of ~45° covering the equatorial ionization anomaly (EIA) crests in the Northern and Southern Hemispheres along the Brazilian longitudes. The locations of ionosondes used in the present study (red dots) along with the locations of pervious F_3 layer observations during geomagnetic storms are displayed in Figure 1. Compared to previous studies, the present study seems to be the first study of the F_3 layer extending to a large latitude range covering both northern and southern EIA crest locations. We especially discuss the role of a super plasma fountain, generated by the eastward PPEF and storm time neutral wind, on the formation and evolution of the storm time F_3 layer in different hemispheres. The present F_3 layer observations will be compared and discussed with previous such observations in section 3.6.

2. Database

The observations from six digital ionosondes at different locations along the Brazilian longitudes are used in this study. Figure 1 shows the geographic locations of the digisondes. Table 1 lists their geographic and geomagnetic coordinates. The locations of the digisondes cover a latitudinal span from ~20°S to 25°N dip latitudes and covers the EIA crest locations in the north and south. The digisonde data are obtained from the University of Massachusetts Lowel (UML) Digital Ionogram Database network (http://ulcar.uml.edu/DIDBase/; http://spase.info/SMWG/Observatory/GIRO), Reinisch and Galkin (2011). The ionograms from all stations are manually scaled using SAO explorer software (Khmyrov et al., 2008) to derive the h′F and f_oF_2 values. The hmF values are obtained from the electron density profile calculated using SAO. The storm time zonal electric field variations as indicated by the equatorial electrojet (EEJ; e.g., Kane, 1974; Anderson, 2002) are obtained using the H component magnetograms from equatorial station Belem (1.24°S, 311.73°E, −0.07° dip latitude) and off-equatorial station Eusebio (3.88°S, 321.54°E and −7.63° dip latitude). The magnetometer data at Belem are from the African Meridian B-field Education and Research magnetometer network (Yizengaw & Moldwin, 2009) operated by the Boston college and funded by NASA and Air Force Office of Scientific Research (AFOSR). The magnetometer data at Eusebio are from the Estudo e Monitoramento BRAsileiro do Clima Especial (EMBRACE) network (Denardini et al., 2018) operated by the Instituto Nacional de Pesquisas Espaciais of Brazil. The $SymH$ index, solar wind velocity (V), interplanetary magnetic field (IMF), and interplanetary electric field (IEFy) values with 1-min resolution are taken from the Space Physics Data Facility at http://omniweb.gsfc.nasa.gov/ow_min.html. The Universal Time (UT) of the solar wind parameters is suitably shifted to correspond to the UT of ground-based parameters. The wave power index (Wp) related to the wave power of low-latitude Pi2 pulsations which is used to identify the possible presence of substorms is obtained from the website (http://www.isee.nagoya-u.ac.jp/~nose.masahito/s-cubed/insdex.html).

3. Results

3.1. Geomagnetic Storm of 17 March 2015

A coronal mass ejection erupted on 15 March 2015 between 0045 UT and 0200 UT and was flown through as an interplanetary coronal mass ejection hit the Earth's magnetosphere at 0445 UT on 17 March 2015 (http://www.spaceweather.com). This resulted in the most intense geomagnetic storm of the 24th solar cycle, the St. Patrick's Day storm. The storm sudden commencement took place at around 0445 UT

Table 1

List of Digital Ionosondes (DID) Used in the Present Study Along With Their Geographic Coordinates and Dip Latitudes

S. No	Station name and code	Geographic latitude	Geographic longitude	Dip latitude
1	Sao Luis (SALU)	−2.6	315.8	−3.5
2	Fortaleza (FORT)	−3.9	321.6	−8.03
3	Boa Vista (BOAV)	2.8	299.3	9.7
4	Campo Grande (CPGR)	−20.5	305.3	−13.3
5	Cachoera Paulista (CHPI)	−22.7	315.0	−20.1
6	Ramey (RAME)	18.5	292.9	25.9

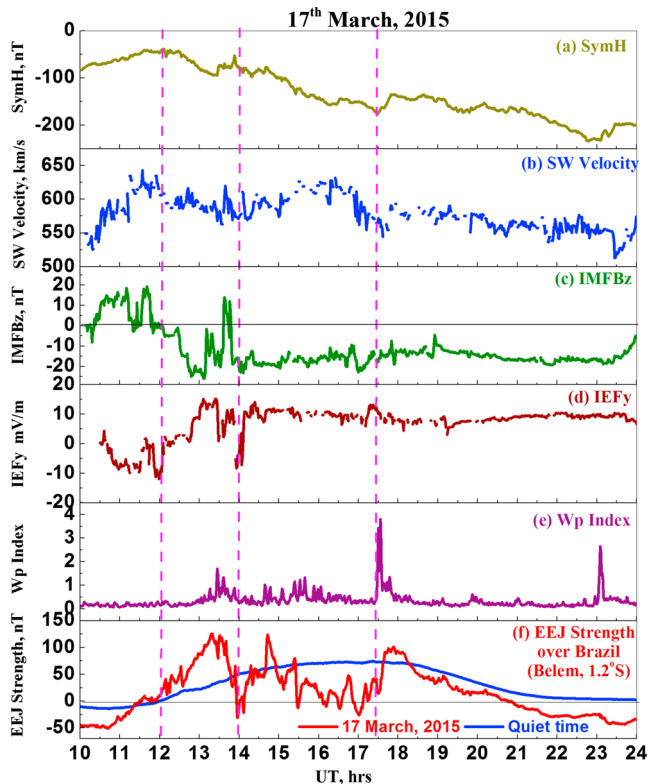*Note.* DID = Digital Ionogram Database

Figure 2. Variations of (a) *SymH* index, (b) solar wind velocity, (c) IMF B_z, (d) IEFy, (e) *Wp* Index and (f) EEJ strength over Brazil during the main phase of the geomagnetic storm (1000 to 2000 UT) on 17 March 2015. SW = solar wind; IMF = interplanetary magnetic field; IEFy = interplanetary electric field; EEJ = equatorial electrojet.

followed by a long MP lasting until 2300 UT. It has an intensity (or minimum *Dst* or DstMin) of −223 nT and impulse strength (or mean *Dst* during MP; Balan et al., 2016) of −113 nT. During the MP, the Brazilian sector (LT = UT − 3) was on the dayside and facilitated to investigate the storm time response of equatorial dynamics and distinct features like the F_3 layer.

Figure 2 presents the time histories of (a) *SymH* index (b) solar wind (SW) velocity, (c) IMF (B_z), (d) IEFy, (e) *Wp* Index, and (f) EEJ strength over Brazil during the MP of the storm from 1000 to 2400 UT (07 to 21 LT in Brazil) on 17 March 2015. The enhanced solar wind velocity (Figure 2b) reaching a maximum of ~625 m/s indicates a strong solar wind-magnetosphere interaction. The IMF B_z (Figure 2c) turns southward at around 1200 UT followed by a rapid negative excursion around 1240 UT. The IEFy (Figure 2d) is negative from 1000 UT and turns positive at 1200 UT with a strong enhancement at 1240 UT in coincidence with the southward excursion of IMF B_z. The EEJ variations over the Brazilian sector (Figure 2f) shows that the zonal electric field is initially westward and becomes eastward (positive EEJ) at 1200 UT with a strong enhancement compared to the quiet time level around 1240 UT. These observations indicate that, during the southward excursion of IMF B_z, the IEFy caused a prompt penetration leading to the enhanced zonal electric field (or EEJ strength of ~100 nT) over the quiet time background. After 1300 UT, the IMF B_z exhibits several fluctuations and a momentary northward turning while the IEFy and EEJ are positive and strong.

To see the possible presence of substorms, variations of the wave power index (*Wp*) are presented in Figure 2e. The wave power of low-latitude Pi2 pulsations has close relation to the substorm onset which can be identified by a sudden increase in the *Wp* index (Nosé et al., 2009, 2012). It can be seen (from Figure 2) that there is an increase in the *Wp* index around 1330 UT showing the presence of a substorm, as also reported by Tulasi Ram et al. (2016). IEFy and EEJ show a strong positive (eastward) phase between 1200 and 1400 UT during MP. This enhanced EEJ phase is termed as PPEF-1 phase (Venkatesh et al., 2017). Later at 1725 UT, the EEJ shows a secondary enhancement (~50 nT over the background) without significant variations in the interplanetary electric and magnetic fields. It can be noticed that the *Wp* index shows a coherent sharp peak indicating the onset of a substorm. This second positive excursion in EEJ following the substorm is denoted as PPEF phase-2 (Venkatesh et al., 2017). Except for the two eastward PPEF phases, the EEJ compared to its quiet variation is generally weak during MP. It indicates the presence of a long-lasting westward disturbance dynamo electric field (DDEF) during the MP, as reported by Huang et al. (2016). The rest of the manuscript focuses on the onset and evolution of F_3 layer at different latitudes in response to the two PPEF phases.

3.2. Examples of F_3 Layer

Figure 3 shows typical ionograms displaying distinct F_3 layer observed over the six locations during the strong PPEF-1 phase. The UT and corresponding local times (LT) are noted. Clear F_3 layer is observed over a large latitudinal extent of ~45° covering the EIA crests in the Northern and Southern Hemispheres. As expected (Balan et al., 1998), the layer is least distinct close to the equator (SALU) and most distinct at off-equatorial locations (BOAV and CPGR). The (virtual) height of the layer decreases while its critical frequency increases with latitude up to the highest latitude (RAME), which indicates that the EIA crest has moved to the location of RAME (25.9° dip latitude) or beyond during the strong PPEF-1 phase. Figure 4 shows a similar set of ionograms over the six locations during the weak PPEF-2 phase. The presence of the F_3 layer is similar to that during PPEF-1 phase, but its latitudinal extend is short (note the absence of F_3 layer at RAME, Figure 4). The EIA crest location also moved to lower latitude (CPGR) where the critical frequency is maximum.
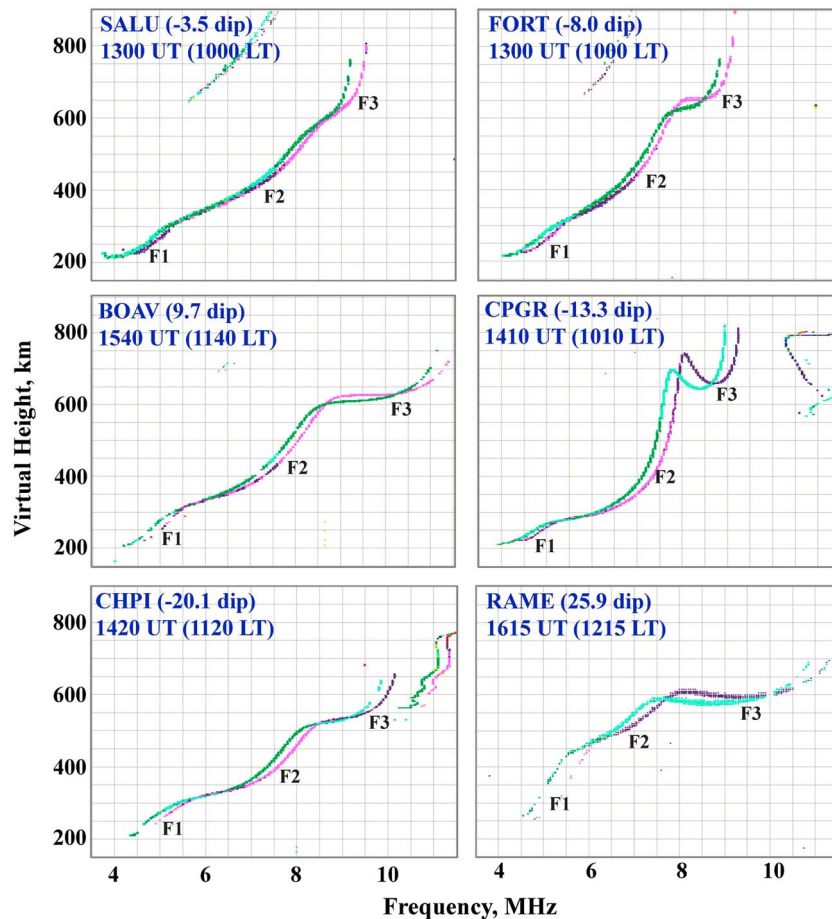
Figure 3. A set of ionograms showing the presence of F_3 layer at six different locations during the PPEF-1 phase during the main phase of the 17 March 2015 storm. PPEF = prompt penetration electric field.

A comparison of Figures 3 and 4 shows clear dependence of F_3 layer on the PPEF phases. It also indicates significant north-south asymmetry in F_3 layer. More distinct F_3 layers occur at higher latitudes during stronger PPEF (Figure 3) than during the weaker PPEF (Figure 4). The strongest critical frequency also corresponds to higher latitudes (RAME, 25.9°N; CHPI, −20.1°S) during the stronger PPEF (Figure 3) than during weaker PPEF (Figure 4; CPGR, −13.3°S). These observations indicate the combined action of plasma fountain due to PPEF and storm time neutral wind on the F_3 layer occurrence. In addition to the difference in the intensity of the two PPEF phases, the differences in F_3 layer during these phases (Figures 3 and 4) involve their local time difference (PPEF-1 at around 1200 UT, 0900 LT and PPEF-2 at around 1725 UT, 1425 LT). The local times of the ionograms shown are until 1215 LT in Figure 3 and 1650 LT in Figure 4.

3.3. F_3 Layer Duration

To study the duration of F_3 layer at different latitudes, we obtained the time duration of F_3 layer occurrence at all six locations. Figure 5 shows a plot of the F_3 layer durations as a function of UT and dip latitude. The horizontal bars of different colors give the durations at different locations. The F_3 layer started occurring at or after 1230 UT (30 min after the beginning of PPEF-1) at all six locations during the PPEF-1 phase (left bars). After its disappearance, a new F_3 layer occurred at or after 1730 UT during PPEF-2 phase at all locations (right bars) except at the highest latitude location (RAME). It is interesting to note that the onset time and duration follow clear (and similar) latitudinal patterns during both PPEF phases. The layer occurred earlier at the equator (SALU) and later at higher latitudes. At the highest latitude locations, the layer actually occurred after the end of the PPEF phases (RAME during PPEF-1 and BOAV during PPEF-2). The
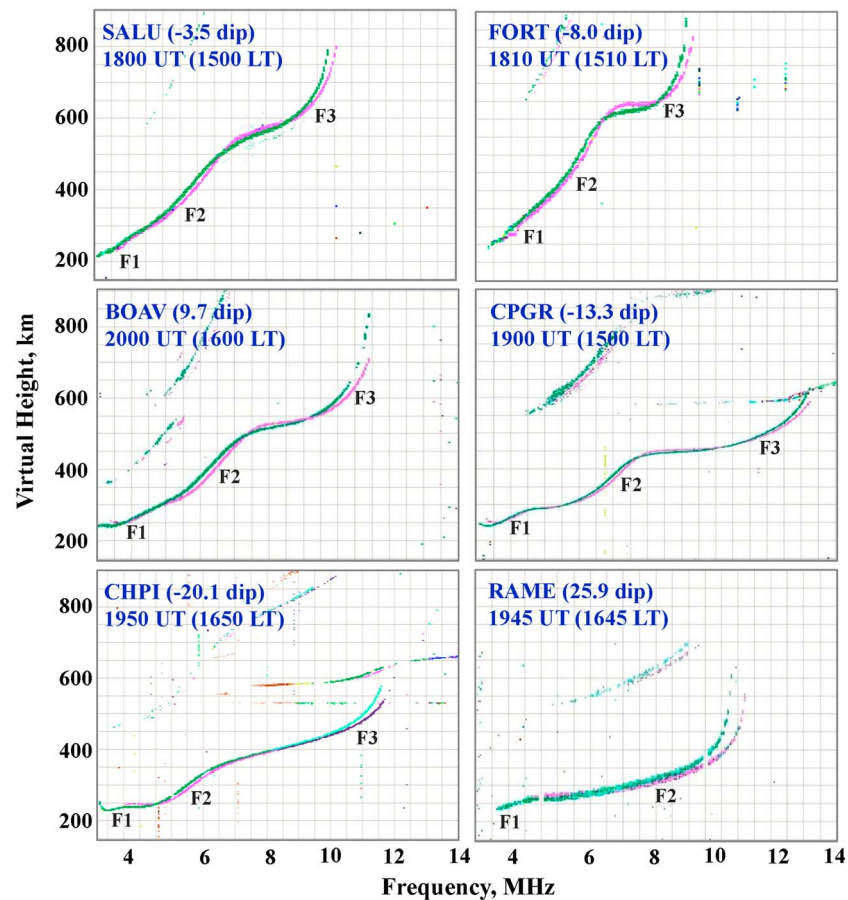
Figure 4. A set of ionograms showing the presence of F_3 layer, except at the higher latitude location RAME during the PPEF-2 phase during the main phase of the 17 March 2015 storm. PPEF = prompt penetration electric field.
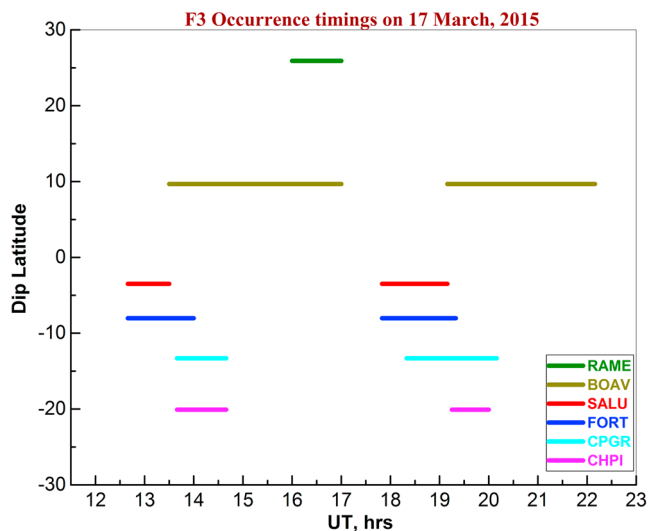
duration in general increases with latitude up to a certain latitude (note the longest bars at around $\pm 10°$ dip latitude) and then decreases during both PPEF phases. There are also clear north-south differences in the onset time and durations of F_3 layer. It occurs earlier in the Southern Hemisphere but lasts longer in the Northern Hemisphere (compare the bars at around $\pm 10°$ latitudes). These features of the F_3 layer indicate the effects of the super plasma fountain due to eastward PPEF and north-south asymmetry of storm time neutral wind.

3.4. Ionospheric Height and Peak Density Variations

In order to study the ionospheric height and density characteristics during F_3 layer occurrence, the variations of F layer virtual base height (h′F) and peak height (hmF) during the MP (1000–2400 UT, 0700–2100 LT) on 17 March 2015 are computed and presented in Figure 6. The six panels in the left column correspond to h′F at the six locations, and those in the right column correspond to hmF. The storm time variations (red curves) are also compared with quiet time variations (blue curves). The quiet time values correspond to the mean of the parameters on five quiet days before the geomagnetic storm. The green color horizontal bars indicate the durations of F_3 layer occurrence at different locations. It is clearly seen from this figure that, compared to quite conditions, the
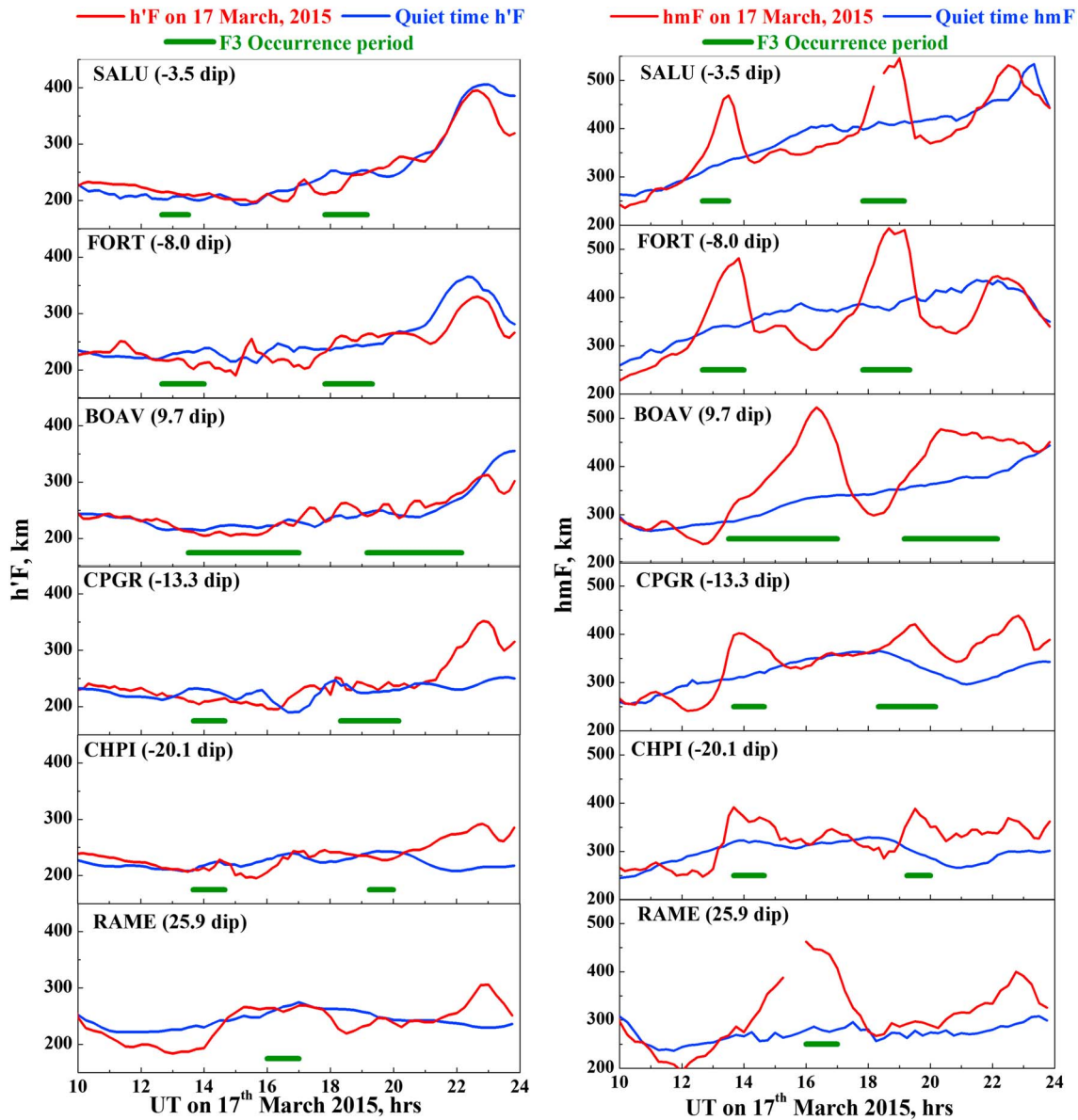

Figure 5. Plot showing the time duration of F_3 layer occurrence at different locations during the two PPEF phases. PPEF = prompt penetration electric field.

Figure 6. Variations of F layer virtual height (h′F, left column) and peak height (hmF, right column) at six different locations. The blue and red curves indicate quiet time and storm time variations, respectively. The green color horizontal bars show the durations of F_3 layer occurrences.

base height (left panels) does not show any significant changes during F_3 layer (and PPEF phases) at any location.

The peak height (right column) on the other hand enhanced significantly and showed clear latitude dependence during F_3 layer (PPEF) phases. Over the equatorial stations SALU and FORT, the hmF rapidly enhanced reaching up to 465 and 550 km, respectively, during PPEF-1 and PPEF-2 phases. Beyond the equatorial locations, the height raise is smaller at the stations located in the Southern Hemisphere (CPGR and CHPI), than those in the Northern Hemisphere (BOAV and RAME). The height raise is smaller during the weaker PPEF-2 phase especially at off equatorial locations (BOAV, CPGR, CHPI and RAME). These observations again indicate the combined effect of PPEF and equatorward wind.

Figure 7 shows variations of ionospheric peak electron density (Nmax) during 1000–2400 UT on the storm day (17 March 2015, red curves) at all six locations, which are also compared with the variations under quite conditions (blue curves). Unlike hmF, Nmax decreases during F_3 layer formation (horizontal green bars) at
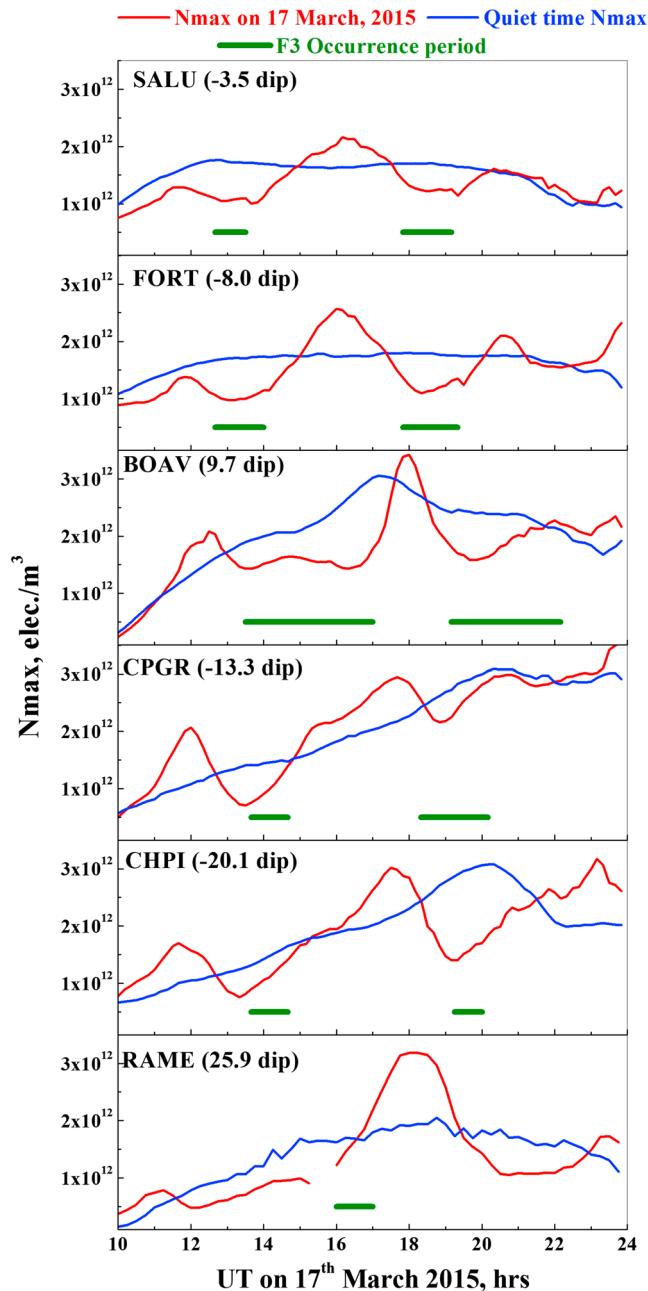
Figure 7. Variations of F layer peak density (Nmax) at six different locations. The red and blue curves indicate storm time and quiet time variations, respectively. The green color horizontal bars show the durations of F_3 layer occurrences.

all latitudes (Figure 7), more significantly at equatorial latitudes. This is expected because when the ionosphere is uplifted or raised in height, the ionospheric plasma gets redistributed upward along the field lines causing Nmax to decrease. The Nmax depletion along with hmF enhancement (Figure 6) in the northern low-latitude stations (BOAV and RAME) lasts longer compared to those in the southern low-latitude stations (CPGR and CHPI). This indicates the effects of (geomagnetically) symmetric PPEF and asymmetric neutral wind.

3.5. F_3 Layer Evolution

The sequence of ionograms, shown in Figure 8 (one row for each location), illustrates the evolution of F_3 layer during the PPEF-1 phase. In each row, the first ionogram corresponds to the one just before the onset of F_3 layer and the last ionogram corresponds to the one immediately after the disappearance of the F_3 layer. The red dotted arrow lines follow the variation of the F_3 layer base virtual height in the ionogram trace. As shown by the arrows, the F_3 layer at the equatorial locations (SALU, FORT, and BOAV) drifted upward to the topside ionosphere due to the dominating effect of the eastward PPEF and disappeared from the ionogram. At the low-latitude locations (CPGR, CHPI, and RAME), the F_3 layer drifts downward as indicated by the base height (red color arrow lines) and merged with the F_2 layer. Similar evolution of F_3 layer was observed during the weak PPEF-2 phase (Figure not shown). Section 4 below discusses the observations.

3.6. Comparison With Earlier Studies on F_3 Layer Occurrence

The F_3 layer occurrence due to PPEF during geomagnetic storms have been reported in the literature (Balan et al., 2008; Batista et al., 2017; Klimenko et al., 2011 ; Lin et al., 2009 ; Paznukhov et al., 2007 ; Sreeja et al., 2009). Table 2 shows a comparison of the F_3 layer occurrence and its latitudinal extent reported in earlier studies and the present study. Table 2 lists the previous studies, the geomagnetic storm with its peak negative Dst value, the number of observing stations, latitudinal extent of F_3 layer occurrence, and the main findings from the studies. Majority of the earlier studies (Klimenko et al., 2011; Lin et al., 2009; Paznukhov et al., 2007; Sreeja et al., 2009) reported the storm time F_3 layer using only a single equatorial station. Balan et al. (2008) have shown the F_3 layer occurrence at three stations spanning from the equator to southern low-latitudes of 11.6°S. Later, Batista et al. (2017) presented the F_3 layer occurrence at two conjugate stations at 9.7°N and 13.3°S dip latitudes. In general, the F_3 layer occurrences over equatorial latitudes during storm times are explained due to rapid uplift of F layer by eastward PPEF owing to the southward turning of IMF B_z. In the present study, the F_3 layer extended over ~45° latitudinal belt covering the EIA crest reg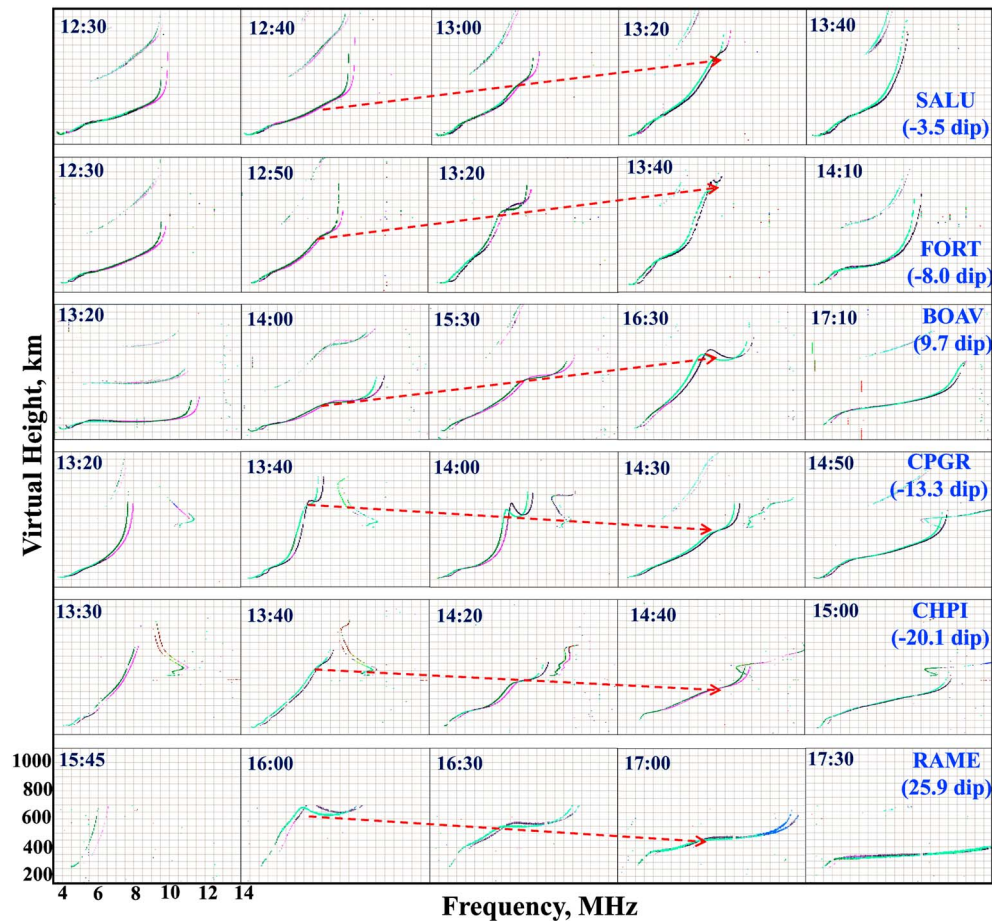ions in both hemispheres over the Brazilian sector. This is the largest latitudinal extent of F_3 layer occurrence that has ever been reported. During the super geomagnetic storm of 9 November 2004, rapid F layer uplift took place at several low-latitude stations due to PPEF (with the southward turning of IMF B_z) including RAME (Paznukhov et al., 2007); however, the F_3 layer occurred only at the equator. During the present storm, in addition to the rapid F layer elevation, the F_3 layer extends from the equator to beyond the EIA crests in both hemispheres to the location of RAME (26°N dip latitude). The combined action of storm time PPEF and disturbed winds for the latitudinal extension and hemispheric differences of the occurrence and evolution of storm time F_3 layer is discussed in the next section.

Figure 8. Sequences of ionograms depicting the onset and evolution of F_3 layer characteristics at different latitudes during PPEF-1 phase. The red color arrow lines indicate the variations with time of the F_3 layer base height. PPEF = prompt penetration electric field.

Table 2
Latitudinal Extent and Other Main Features of F_3 Layer Reported During Geomagnetic Storms

S. No	Study	Storm	Latitude extent of F_3 layer occurrence	Main findings
1	Present Study	17 March 2015 DstMin −223 nT	Six stations 22.7°S to 25°N dip	F_3 layer extends beyond the EIA crests, with significant hemispheric differences in the occurrence, duration and critical frequency.
2	Paznukhov et al. (2007)	9 November 2004 DstMin −263 nT	One station 1°N dip	Strong F_3 layer occurred over the equator due to fast up lift of the F region during a large IMF B_z southward event.
3	Balan et al. (2008)	7–11 November 2004 DstMin −373 nT	Three stations 11.6°S to 1°N dip	Strong F_3 layer occurred around the equator. It is attributed to strong the upward $E \times B$ drift (or eastward PPEF) during the large IMF B_z southward event.
4	Sreeja et al. (2009)	4–6 October 2000 DstMin −182 nT	One station 0.5°N dip	The unexpected F_3 layer observed at dawn is attributed to strong eastward PPEF.
5	Lin et al. (2009)	29 October 2003 DstMin −353 nT	One station 1°N dip	The mechanism of storm time F_3 layer is similar to that of quiet time F_3 layer.
6	Klimenko et al. (2011)	9–14 September 2005 DstMin −139 nT	One station 1°N dip	Geomagnetic storms affect the formation, existence, duration, and number of additional layers in the equatorial ionosphere.
7	Batista et al. (2017)	17 March 2015 DstMin −222 nT	Two conjugate stations 9.7° N, 13.3° S dip	The thickness parameter (B0) is a good proxy for F_3 layer occurrence. The layer during disturbed periods lasts longer in the hemisphere of faster equatorward effective meridional wind.

Note. IMF = interplanetary magnetic field

4. Discussion and Concluding Remarks

The most important results presented in section 3 can be outlined as follows:

1. The F_3 layer occurred during both PPEF phases over a large latitudinal extent from ~20°S to ~25°N dip latitudes covering the EIA crests in both hemispheres except at the highest latitude station RAME during the weak PPEF-2 phase.
2. The F_3 layer started occurring earlier at the equator and later at higher latitudes in both hemispheres.
3. The F region peak height was rapidly uplifted (or raised) and the peak density reduced during F_3 layer occurrence. The F region base height, however, did not experience any significant change.
4. The F_3 layer evolved in such a way that it ascended to the topside ionosphere at lower latitudes (<10° dip latitude) while at higher latitudes the F_3 layer descended with time and merged with the F_2 layer.
5. The F_3 layer was more distinct and stronger, and lasted longer in the Northern Hemisphere than in the Southern Hemisphere.

These storm time modifications of the F layer vertical structure and F_3 layer occurrence include the combined effects of the (1) eastward PPEF, (2) mechanical effects of storm time asymmetric equatorward neutral wind (ENW), (3) DDEF, and (4) natural variation of the ionosphere in the absence of PPEF and wind. PPEF is symmetric with respect to the geomagnetic equator, while ENW and hence DDEF are generally asymmetric. The ionospheric F layer response at different locations and different times depends on which factor dominates over the other.

The eastward PPEF acts as the main driver for rapid F layer uplift centered around the equator generating super plasma fountain. During both PPEF phases, the super plasma fountain results in the development of strong EIA crests and positive storm effects (Astafyeva et al., 2015; Nava et al., 2016; Venkatesh et al., 2017). During the strong PPEF-1, there is a poleward departure of southern anomaly crest upto ~40°S geographic latitudes (Venkatesh et al., 2017). The storm time super plasma fountain led to the onset of the F_3 layer first at the equatorial location (SALU) following the PPEF phases and later at higher latitudes (Figure 5).

The horizontal winds can contribute to the field-aligned transport of ionospheric plasma due to the inclination (I) and declination (D) angles of field lines. The effective wind that can cause upward/downward transport of plasma along filed lines is given by the expression

$$U_{\text{eff}} = \left(U_\theta \, \cos D \pm U_\varphi \, \sin D \right) \, \cos I \, \sin I$$

where D and I are the magnetic declination and inclination angles, respectively, and U_θ (equator ward) and U_φ (eastward positive) are the meridional and zonal wind velocities (Titheridge, 1995). Hence, the mechanical effects of ENW (a) reduce or (stop) downward diffusion along the field lines and (b) raise the ionospheric height through U_{eff} (Balan et al., 2011).

Huang et al. (2016) reported that the disturbance dynamo process during this storm initiated 3–4.7 hr after the MP onset and lasted for 31 hr. Using the satellite observations from DMSP and C/NOFS constellations, Hairston et al. (2016) have shown the presence of strong disturbance fields and intense meridian flows after the storm onset and reported that they affected the equatorial ionosphere. The DDEF would have been strongly westward during the whole MP, except during the PPEF phases, as understood from the lower than normal EEJ strength (Figure 2). Tulasi Ram et al. (2016) reported that the meridional wind becomes southward around 1400 UT with a large equatorward wind surge (200–300 m/s) during the MP of the storm in the nightside over Japanese sector. Similarly, strong ENW surge (>200 m/s) in the dayside (American sector) is reported by Zhang et al. (2017) using the Millstone Hill radar observations. The ENW and DDEF could have been in action during the present PPEF phases, as they occurred several hours after the storm onset.

The PPEF induced super plasma fountain enhances the pumping of ionization away from the equator, and the coexisting ENW reduces the downward diffusion and raise the ionospheric height at the low latitudes. Thus, the combined effect of strong PPEF and ENW can account for the occurrence of F_3 layer over a large extent up to about 25° dip latitudes. In other words, F_3 layer might have occurred at latitudes even beyond RAME (~25° dip latitude) during the strong PPEF-1 phase (Figure 3).

The dominant effect of PPEF at and near the equatorial locations (SALU, FORT, and BOAV) caused the F_3 layer there to ascend to the topside ionosphere (Figure 8). The peak height enhancement is larger at equatorial ($< \pm 10°$ dip latitudes) and higher latitudes ($> \pm 20°$ dip latitudes) and smaller at intermediate latitudes (between $\pm 10°$ and $\pm 20°$ dip latitudes; Figure 6). While the ionospheric peak height increases due to PPEF, the peak density decreases (Figures 6 and 7) because the ionospheric plasma distributes along the field lines. Because the effect of ENW to raise the ionospheric height is weak and slow and the ionospheric peak height naturally reduces rapidly with increasing latitude, the F_3 layer base height at off equatorial locations decreases with time and F_3 layer merges with F_2 layer during both PPEF phases.

The uplifting effect of PPEF decreases with increasing dip angle (I). PPEF also accelerates downward diffusion along the geomagnetic field lines. This enhanced downward diffusion is reduced (or stopped) by the effect (a) of the ENW at off equatorial locations where F_3 layer becomes more distinct (BOAV and CPGR) compared to those at lower latitudes (Figures 3 and 4). The layer also becomes more distinct and stronger in that hemisphere where the ENW is faster. In the present case, the ENW would have been faster in the Northern Hemisphere as seen from the stronger F_3 layer and critical frequency in that hemisphere (BOAV and RAME; Figure 3). Evidence for a stronger ENW in the Northern Hemisphere during the 17 March 2015 storm period was given in Batista et al. (2017) comparing the F region heights at two stations along the same magnetic meridian in Brazilian longitudes (BOAV and CPGR).

The present study, using simultaneous ionosonde observations from six different locations, reports for the first time the occurrence of storm time F_3 layer over a large latitudinal extent of $\sim 45°$ covering EIA crests in both hemispheres. It is further inferred that, while the PPEF induced super plasma fountain provides major forcing from the equator, the combined action of PPEF and storm time ENW together contribute for the formation, evolution, and hemispheric asymmetries of storm time F_3 layer at different latitudes.

References

Anderson, D. (2002). Estimating daytime vertical ExB drift velocities in the equatorial F-region using ground-based magnetometer observations. *Geophysical Research Letters*, *29*(12), 1596. https://doi.org/10.1029/2001GL014562

Astafyeva, E., Zakharenkova, I., & Förster, M. (2015). Ionospheric response to the 2015 St. Patrick's Day storm: A global multi-instrumental overview. *Journal of Geophysical Research: Space Physics*, *120*, 9023–9037. https://doi.org/10.1002/2015JA021629

Balan, N., Bailey, G. J., Abdu, M. A., Oyama, K. I., Richards, P. G., MacDougall, J., & Batista, I. S. (1997). Equatorial plasma fountain and its effects over three locations: Evidence for an additional layer, the F 3 layer. *Journal of Geophysical Research*, *102*(A2), 2047–2056. https://doi.org/10.1029/95JA02639

Balan, N., Batista, I. S., Abdu, M. A., Bailey, G. J., Watanabe, S., MacDougall, J., & Sobral, J. H. A. (2000). Variability of an additional layer in the equatorial ionosphere over Fortaleza. *Journal of Geophysical Research*, *105*(A5), 10,603–10,613. https://doi.org/10.1029/1999JA000020

Balan, N., Batista, I. S., Abdu, M. A., MacDougall, J., & Bailey, G. J. (1998). Physical mechanism and statistics of occurrence of an additional layer in the equatorial ionosphere. *Journal of Geophysical Research*, *103*(A12), 29,169–29,181. https://doi.org/10.1029/98JA02823

Balan, N., Batista, I. S., Tulasi Ram, S., & Rajesh, P. K. (2016). A new parameter of geomagnetic storms for the severity of space weather. *Geoscience Letters*, *3*(1), 3. https://doi.org/10.1186/s40562-016-0036-5

Balan, N., Thampi, S. V., Lynn, K., Otsuka, Y., Alleyne, H., Watanabe, S., et al. (2008). F_3 layer during penetration electric field. *Journal of Geophysical Research*, *113*, A00A07. https://doi.org/10.1029/2008JA013206

Balan, N., Yamamoto, M., Sreeja, V., Batista, I. S., Lynn, K. J. W., Abdu, M. A., et al. (2011). A statistical study of the response of the dayside equatorial F_2 layer to the main phase of intense geomagnetic storms as an indicator of penetration electric field. *Journal of Geophysical Research*, *116*, A03323. https://doi.org/10.1029/2010JA016001

Batista, I. S., Abdu, M. A., MacDougall, J., & Souza, J. R. (2002). Long term trends in the frequency of occurrence of the F_3 layer over Fortaleza, Brazil. *Journal of Atmospheric and Solar-Terrestrial Physics*, *64*(12–14), 1409–1412. https://doi.org/10.1016/S1364-6826(02)00104-9

Batista, S. I., Candido, C. M. N., Souza, J. R., Abdu, M. A., de Araujo, R. C., Resende, L. C. A., & Santos, A. M. (2017). F3 layer development during quiet and disturbed periods as observed at conjugate locations in Brazil: The role of the meridional wind. *Journal of Geophysical Research: Space Physics*, *122*, 2361–2373. https://doi.org/10.1002/2016JA023724

Denardini, C. M., Chen, S. S., Resende, L. C. A., Moro, J., Bilibio, A. V., Fagundes, P. R., et al. (2018). The Embrace Magnetometer Network for South America: Network description and its qualification. *Radio Science*, *53*, 288–302. https://doi.org/10.1002/2017RS006477

Fagundes, P. R., Klausner, V., Sahai, Y., Pillat, V. G., Becker-Guedes, F., Bertoni, F. C. P., et al. (2007). Observations of daytime F_2-layer stratification under the southern crest of the equatorial ionization anomaly region. *Journal of Geophysical Research*, *112*, A04302. https://doi.org/10.1029/2006JA011888

Hairston, M., Coley, W. R., & Stoneback, R. (2016). Responses in the polar and equatorial ionosphere to the March 2015 St. Patrick Day storm. *Journal of Geophysical Research: Space Physics*, *121*, 11,213–11,234. https://doi.org/10.1002/2016JA023165

Huang, C.-S., Wilson, G. R., Hairston, M. R., Zhang, Y., Wang, W., & Liu, J. (2016). Equatorial ionospheric plasma drifts and O^+ concentration enhancements associated with disturbance dynamo during the 2015 St. Patrick's Day magnetic storm. *Journal of Geophysical Research: Space Physics*, *121*, 7961–7973. https://doi.org/10.1002/2016JA023072

Jenkins, B., Bailey, G. J., Abdu, M. A., Batista, I. S., & Balan, N. (1997). Observations and model calculations of an additional layer in the topside ionosphere above Fortaleza, Brazil. *Annales Geophysicae*, *15*(6), 753–759. https://doi.org/10.1007/s00585-997-0753-3

Kane, R. P. (1974). Relation between the strength of the Sq current system and its focus position. *Proceedings - Mathematical Sciences*, *80*(1), 17–25. https://doi.org/10.1007/BF03046669

Khmyrov, G. M., Galkin, I. A., Kozlov, A. V., Reinisch, B. W., Mcelroy, J., Khmyrov, G. M., et al. (2008). Exploring digisonde ionogram data with SAO-X and DIDBase. *AIP Conference Proceedings*, *974*(1), 175–185.

Klimenko, M. V., Klimenko, V. V., Ratovsky, K. G., Goncharenko, L. P., Sahai, Y., Fagundes, P. R., et al. (2011). Numerical modeling of ionospheric effects in the middle- and low-latitude *F* region during geomagnetic storm sequence of 9–14 September 2005. *Radio Science*, *46*, RS0D03. https://doi.org/10.1029/2010RS004590

Kuai, J., Liu, L., Liu, J., Sripathi, S., Zhao, B., Chen, Y., et al. (2016). Effects of disturbed electric fields in the low-latitude and equatorial ionosphere during the 2015 St. Patrick's Day storm. *Journal of Geophysical Research: Space Physics*, *121*, 9111–9126. https://doi.org/10.1002/2016JA022832

Lin, C. H., Richmond, A. D., Liu, J. Y., Bailey, G. J., & Reinisch, B. W. (2009). Theoretical study of new plasma structures in the low-latitude ionosphere during a major magnetic storm. *Journal of Geophysical Research*, *114*, A05303. https://doi.org/10.1029/2008JA013951

Lynn, K. J. W., Harris, T. J., & Sjarifudin, M. (2000). Stratification of the F_2 layer observed in Southeast Asia. *Journal of Geophysical Research*, *105*(A12), 27,147–27,156. https://doi.org/10.1029/2000JA900056

Nava, B., Rodríguez-Zuluaga, J., Alazo-Cuartas, K., Kashcheyev, A., Migoya-Orué, Y., Radicella, S. M., et al. (2016). Middle- and low-latitude ionosphere response to 2015 St. Patrick's Day geomagnetic storm. *Journal of Geophysical Research: Space Physics*, *121*, 3421–3438. https://doi.org/10.1002/2015JA022299

Nosé, M., Iyemori, T., Takeda, M., Toh, H., Ookawa, T., Cifuentes-Nava, G., et al. (2009). New substorm index derived from high-resolution geomagnetic field data at low latitude and its comparison with AE and ASY indices. In Proc. XIII IAGA Workshop.

Nosé, M., Iyemori, T., Wang, L., Hitchman, A., Matzka, J., Feller, M., et al. (2012). *Wp* index: A new substorm index derived from high-resolution geomagnetic field data at low latitude. *Space Weather*, *10*, S08002. https://doi.org/10.1029/2012SW000785

Paznukhov, V. V., Reinisch, B. W., Song, P., Huang, X., Bullett, T. W., & Veliz, O. (2007). Formation of an F_3 layer in the equatorial ionosphere: A result from strong IMF changes. *Journal of Atmospheric and Solar-Terrestrial Physics*, *69*(10-11), 1292–1304. https://doi.org/10.1016/j.jastp.2006.08.019

Rama Rao, P. V. S., Niranjan, K., Prasad, D. S. V. V. D., Brahmanandam, P. S., & Gopikrishna, S. (2005). Features of additional stratification in ionospheric F_2 layer observed for half a solar cycle over Indian low latitudes. *Journal of Geophysical Research*, *110*, A04307. https://doi.org/10.1029/2004JA010646

Reinisch, B. W., & Galkin, I. A. (2011). Global Ionospheric Radio Observatory (GIRO). *Earth, Planets and Space.*, *63*(4), 377–381. https://doi.org/10.5047/eps.2011.03.001

Sreeja, V., Balan, N., Sudha, R., Pant, T. K., Sridharan, R., & Bailey, G. J. (2009). Additional stratifications in the equatorial *F* region at dawn and dusk during geomagnetic storms: Role of electrodynamics. *Journal of Geophysical Research*, *114*, A08309. https://doi.org/10.1029/2009JA014373

Sreeja, V., Ravindran, S., & Pant, T. K. (2010). Features of the F_3 layer occurrence over the equatorial location of Trivandrum. *Annales Geophysicae*, *28*(9), 1741–1747. https://doi.org/10.5194/angeo-28-1741-2010

Tardelli, A., Fagundes, P. R., Pezzopane, M., Venkatesh, K., & Pillat, V. G. (2016). Seasonal and solar activity variations of F_3 layer and quadruple stratification (StF-4) near the equatorial region. *Journal of Geophysical Research: Space Physics*, *121*, 12,116–12,125. https://doi.org/10.1002/2016JA023580

Tardelli, A., Pezzopane, M., Fagundes, P. R., Venkatesh, K., Pillat, V. G., Cabrera, M. A., & Ezquer, R. G. (2018). Study of the F_3 and StF4 layers at Tucumán near the southern crest of the equatorial ionization anomaly in western South America. *Journal of Geophysical Research: Space Physics.* https://doi.org/10.1002/2017JA024539

Thampi, S. V., Balan, N., Ravindran, S., Pant, T. K., Devasia, C. V., Sreelatha, P., et al. (2007). An additional layer in the low-latitude ionosphere in Indian longitudes: Total electron content observations and modeling. *Journal of Geophysical Research*, *112*, A06301. https://doi.org/10.1029/2006JA011974

Titheridge, J. E. (1995). Winds in the ionosphere—A review. *Journal of Atmospheric and Terrestrial Physics*, *57*(14), 1681–1714. https://doi.org/10.1016/0021-9169(95)00091-F

Tulasi Ram, S., Yokoyama, T., Otsuka, Y., Shiokawa, K., Sripathi, S., Veenadhari, B., et al. (2016). Duskside enhancement of equatorial zonal electric field response to convection electric fields during the St. Patrick's Day storm on 17 March 2015. *Journal of Geophysical Research: Space Physics*, *121*, 538–548. https://doi.org/10.1002/2015JA021932

Uemoto, J., Maruyama, T., Ono, T., Saito, S., Iizima, M., & Kumamoto, A. (2011). Observations and model calculations of the F_3 layer in the Southeast Asian equatorial ionosphere. *Journal of Geophysical Research*, *116*, A03311. https://doi.org/10.1029/2010JA016086

Uemoto, J., Ono, T., Maruyama, T., Saito, S., Iizima, M., & Kumamoto, A. (2007). Magnetic conjugate observation of the F_3 layer using the SEALION ionosonde network. *Geophysical Research Letters*, *34*, L02110. https://doi.org/10.1029/2006GL028783

Venkatesh, K., Tulasi Ram, S., Fagundes, P. R., Seemala, G. K., & Batista, I. S. (2017). Electrodynamic disturbances in the Brazilian equatorial and low-latitude ionosphere on St. Patrick's Day storm of 17 March 2015. *Journal of Geophysical Research: Space Physics*, *122*, 4553–4570. https://doi.org/10.1002/2017JA024009

Yizengaw, E., & Moldwin, M. B. (2009). African Meridian *B*-field Education and Research (AMBER) array. *Earth, Moon and Planets*, *104*(1-4), 237–246. https://doi.org/10.1007/s11038-008-9287-2

Zain, A. F. M., Abdullah, S., Homam, M. J., Seman, F. C., Abdullah, M., & Ho, Y. H. (2008). Observations of the F_3-layer at equatorial region during 2005. *Journal of Atmospheric and Solar-Terrestrial Physics*, *70*(6), 918–925. https://doi.org/10.1016/j.jastp.2007.12.002

Zhang, S. R., Zhang, Y., Wang, W., & Verkhoglyadova, O. P. (2017). Geospace system responses to the St. Patrick's Day storms in 2013 and 2015. *Journal of Geophysical Research: Space Physics*, *122*, 6901–6906. https://doi.org/10.1002/2017JA024232

Zhao, B., Wan, W., & Liu, L. (2005). Responses of equatorial anomaly to the October–November 2003 superstorms. *Annales Geophysicae*, *23*(3), 693–706. https://doi.org/10.5194/angeo-23-693-2005

Zhao, B., Zhu, J., Xiong, B., Yue, X., Zhang, M., Wang, M., & Wan, W. (2014). An empirical model of the occurrence of an additional layer in the ionosphere from the occultation technique: Preliminary results. *Journal of Geophysical Research: Space Physics*, *119*, 10,204–10,218. https://doi.org/10.1002/2014JA020220